Supplementary Information: Charged Hollow Microgel Capsules

Nabanita Hazra,[a] Janik Lammertz,[a] Andrey Babenyshev,[a] Rebecca Erkes,[a] Fabian Hagemans,[a] Chandeshwar Misra,[a] Walter Richtering,[a] and Jérôme J. Crassous[a,*]

S1 Characterization of the silica seeds

The silica seeds were characterized by dynamic and static light scattering experiments at 20 °C. For the DLS results, the decay rate Γ was plotted against q^2 and linearly fitted Figure S1A. The slope of the fit corresponds to a diffusion coefficient D_0 of $1.00 \pm 0.01\ \mu m^2 s^{-1}$. According to the Stokes-Einstein equation, the hydrodynamic radius R_H was determined at 178 nm. SLS measurements were performed to confirm the spherical shape and to determine the size of the silica seeds. Additionally, the SLS data were fitted with a hard-sphere model (Figure S1B), leading to a radius of 179 nm with a 6% polydispersity in good agreement with the measured R_H.

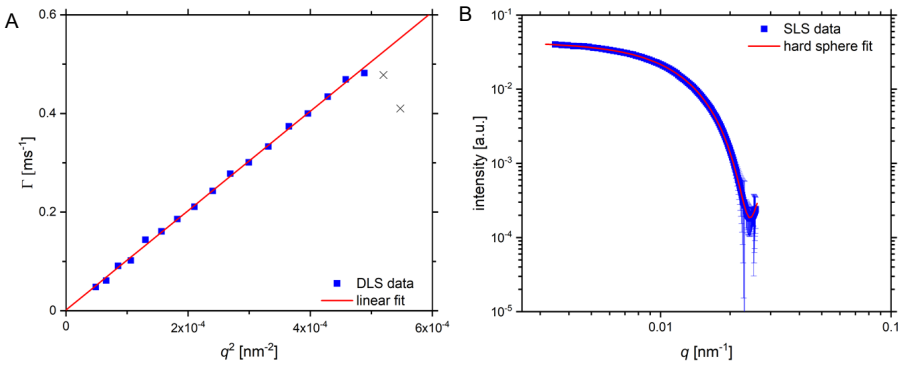

Figure S1 A) Evolution of Γ vs q^2 measured by DLS on a silica precursor dispersion. The slope of the linear fit was used to calculate the hydrodynamic radius of silica seeds. B) SLS data of the seeds fitted with a hard-sphere model.

S2 Atomic force microscopy of neutral and charged core-shell microgels

AFM measurements were performed to probe the morphology of the core-shell and hollow microgels in their dried state. First, core-shell neutral and charged microgels were measured in tapping mode (Figure S2A,B). Both systems appear slightly anisotropic as a consequence of their topology and the cantilever geometry. We did not observe any microgel shell at the glass substrate, probably in respect to the large dimension of the systems and their limited spreading at the surface. The measured transverse and longitudinal height profiles are displayed in Figure S2C,D for a characteristic neutral and charged core-shell microgel. Both look almost identical with a height in the order of the silica core diameter pointing to the presence of a very thin microgel shell. The diameters is about 200 nm larger than the particle maximal height. Such difference could however be related to the cantilever geometry.

Next, the hollow capsules were also measured in the dried state. All glass slides were cleaned by sonication in isopropanol and then activated in O_3/Ozone. This treatment additionally made the glass substrate negatively charged and hydrophilic which leads to a better spreading of drop of the dispersion during sample preparation. Two techniques were used for sample preparation. Dropcasting at room temperature leads to larger variation of the capsule surface topology and lateral and horizontal dimensions as shown in Figure 2 in the main manuscript.

[a] *Institute of Physical Chemistry, RWTH Aachen University, Landoltweg 2, 52074, Aachen, Germany. E-mail: crassous@pc.rwth-aachen.de*

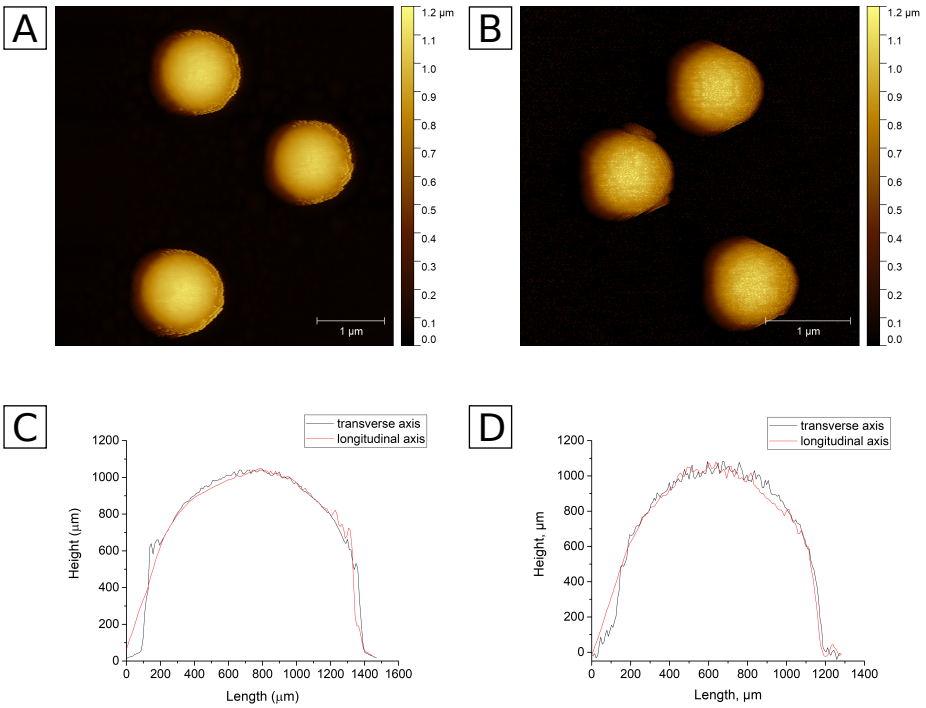

Figure S2 AFM Height micrographs and characteristic transverse and longitudinal height profiles measured on core-shell microgels. (A), (C) correspond to the charged; (B), (D) to the neutral ones.

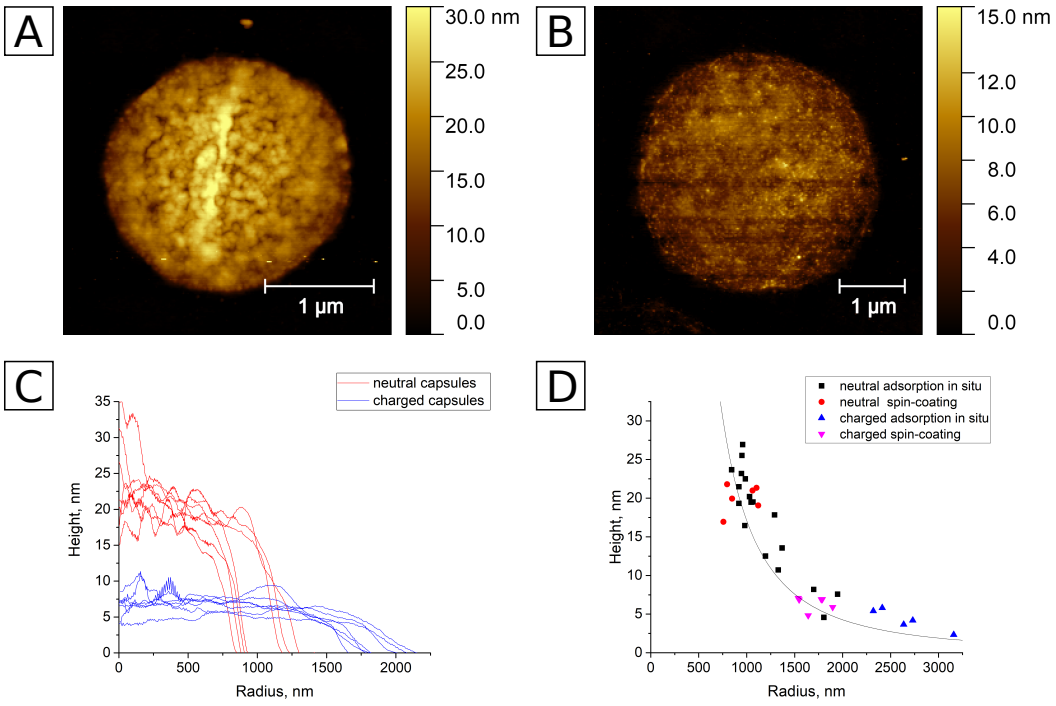

Figure S3 (A) and (B) AFM Height micrographs of neutral and charged hollow capsules measured under dry conditions after spin-coating. (C) Average radial profiles of single neutral (red) and charged (blue) capsules measured under dry conditions after spin-coating. (D) Dependence of height on radius for two types of capsules prepared either by dropcasting or spin-coating.

Spin-coated samples were spin-coated immediately after adding the dispersion. Additional force makes microgels more uniform with less variation in their topology and dimensions compared to dropcasted samples. Only single microgels could be probed in this case and the height micrographs of a characteristic neutral and charged

hollow microgel capsules are shown in Figure S3A and B, respectively. Both systems present appear as circular disks characterized by a much larger radius for the charged capsules as for the neutral one. Conversely, the neutral capsules are much thicker than their charged counterparts. These observations were supported by the average radial height profiles measured on seven capsules for each system (see Figure S3C). Charged capsules are extremely spread with an average height of ≈ 7 nm whereas neutral ones have an average height of ≈ 20 nm. The average height of each measured system is plotted as a function of their radius for the two preparation methods in Figure S3D. The line in Figure S3D) corresponds to a fit of all data considering the inverse proportionality of the height to the squared radius.

S3 Differential dynamic microscopy of charged microgel capsules

DDM relies on the Fourier transform (FT) of a time sequence of micrographs to obtain a power spectrum $g(\vec{q},\tau)$, where $\vec{q}$ refers to the wavevector of the fluctuations being probed and τ is the delay time between two frames recording at a time $t+\tau$ and t, respectively. Considering the difference between the FT of two frames $\widehat{\Delta I}(\vec{q},\tau) = I(\vec{q},t+\tau) - I(\vec{q},t)$, the average power spectrum over τ is defined as follows:

$$g(\vec{q},\tau) = \left\langle \left| \widehat{\Delta I}(\vec{q},\tau) \right|^2 \right\rangle_t \tag{S1}$$

where the brackets denote time averaging. By developing this expression, one obtains the following:

$$g(\vec{q},\tau) = 2\left\langle |I(\vec{q},t)|^2 \right\rangle_t \left[1 - \frac{\langle I(\vec{q},t) I(q,t+\tau)\rangle_t}{\left\langle \left| \widehat{I}(\vec{q},t) \right|^2 \right\rangle_t} \right] \tag{S2}$$

where the more familiar intermediate scattering function $f(\vec{q},\tau)$ can be identified using the Wiener–Khinchin theorem:

$$g(\vec{q},\tau) = A(\vec{q})\,(1 - f(\vec{q},\tau)) \tag{S3}$$

The term $A(\vec{q})$ is here referred to as the amplitude and is related to the scattering intensity of the dispersion being probed and therefore contains both the contribution of the particle form factor, $P(\vec{q})$, and structure factor $S(\vec{q})$ as described in more detail by Lu *et al.*[1] In addition, the τ-independent contribution of the photon, dark, shot and read-out noise $B(q)$ is added, leading to the final expression and main equation of DDM:

$$g(\vec{q},\tau) = A(\vec{q})\big(1 - f(\vec{q},\tau)\big) + B(\vec{q}) \tag{S4}$$

For isotropic systems, the different quantities can be radially averaged. At dilute concentrations for monodisperse systems, $f(q,\tau)$ can be described by a single exponential relaxation function as given by

$$f(q,\tau) = e^{-\tau/\tau_1}, \tag{S5}$$

where τ_1 is the relaxation time which is related to the diffusion coefficient by $D(q) = \tau_1/q^2$. The diffusion coefficients were obtained by fitting the experimentally obtained correlation functions with equations 4 and 5 using our own DDM software (DDM_{Soft})*.[2]

The diffusion coefficient averaged between $q \approx 1.2$ and 2.6 μm^{-1} was determined for temperatures comprised between 20 and 40 °C. $f(q,\tau)$ is plotted against τq^2 for different q-values (Figure SS4). Figure SS4 shows the normalized autocorrelation functions of p(NIPAM-co-IA) capsules at T = 20 °C, I = 10 mM and pH = 3 (a) compared to pH = 9 (b). The $f(q,\tau)$ measurement at different q-values superpose into a mastercurve when $f(q,\tau)$ is plotted as function of τq^2 as expected for diffusive systems. We note that the scattering amplitude shows a minima at lower q values at pH = 9 compared to pH = 3. As $A(q)$ is related to the form factor of the capsules, this could be taken as

* https://github.com/duxfrederic/ddmsoft

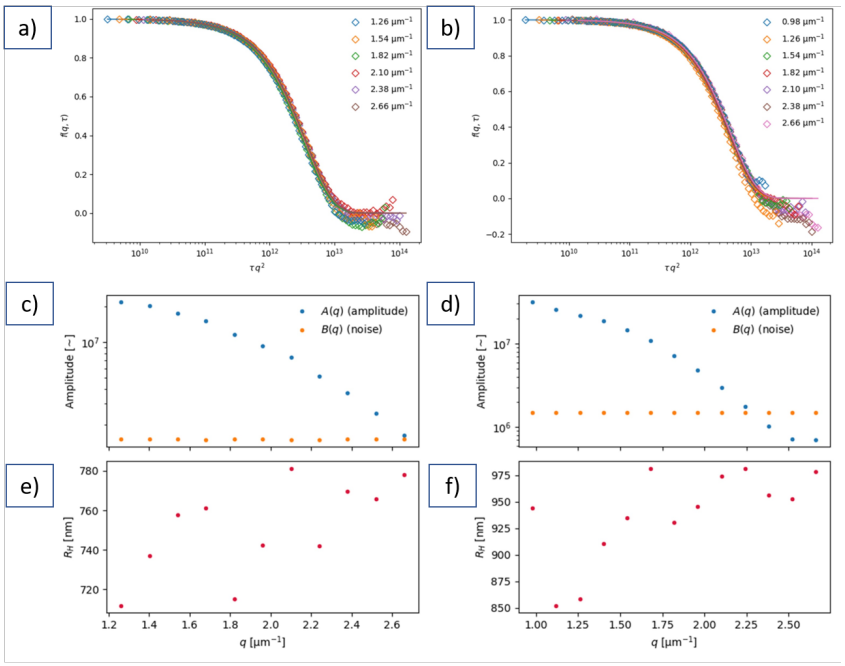

Figure S4 Fitted data of the DDM measurements of p(NIPAM-co-IA) capsules at $T = 20$ °C, $I = 10$ mM and pH = 3 (a, c, e) compared to pH = 9 (b, d, f). The figure compares the autocorrelation functions $f(q, \tau)$ (a, b), the scattering amplitude $A(q)$, and detector noise $B(q)$ (c, d) as well as the hydrodynamic radii R_H as calculated by the Stokes-Einstein equation (e, f).

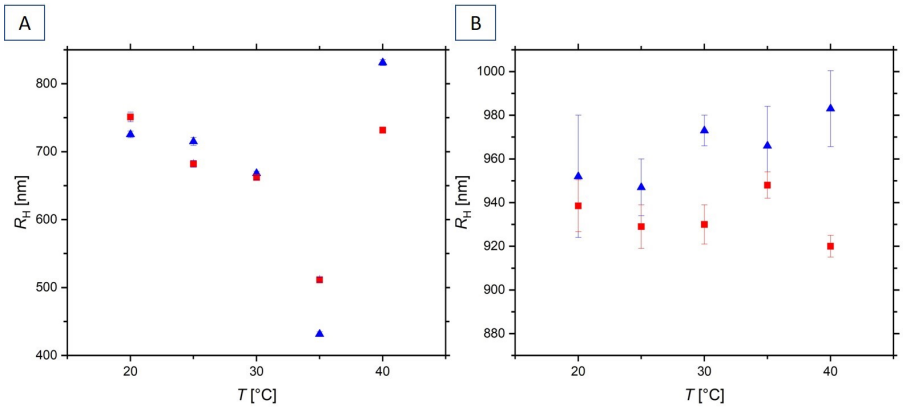

Figure S5 Hydrodynamic radius of p(NIPAM-co-IA) capsules depending on temperature at pH = 3 (A) and pH = 9 (B) and ionic strengths $I = 1$ mM (blue up triangles) and $I = 10$ mM (red squares). The increase of R_H at pH = 3 above 35 °C is ascribed to the coagulation of the systems.

an indication that the capsule size at pH = 9 (d) is larger compared to pH = 3 (c). In contrast, the detector noise is constant over q as expected. The analysis of the temperature dependence of the ionic capsules dependence at pH = 9 and pH = 3 for the two different NaCl concentrations is summarized in Figure SS5 and discussed in more detail in the main manuscript. Note, that we did observe larger variation at pH = 9 than at pH = 3, probably in relation to a larger size polydispersity and/or larger q-dependent fluctuation of the determined R_H values as we are measuring

closer to the minimum of the form factor as discussed in the main manuscript for the DLS measurements.

S4 Dynamic light scattering investigation

The hydrodynamic radius of the different capsules was determined via dynamic light scattering using a first cumulant analysis. Figure S6 illustrates some of the intermediate scattering functions measured at 20°C for neutral (Fig. S6A) and charged capsules (Fig. S6B, C). The charged capsules were measured in a 1 mM buffer at pH = 3 (Fig. S6B) and pH = 9 (Fig. S6C). At first glance, the first cumulant analysis appears to adequately describe the data. However, we noticed that it does not fully capture the fast relaxation measured at short times and low scattering angles for the charged microgels. We believe that such an additional relaxation process may be related to shape fluctuations of the microgel capsules. Similar fluctuations in the case of lipid vesicles have been described with an additional q-independent mode visible when $qR \approx \pi$.[3] The situation here, however, is much more complex as we are considering the fluctuation of an elastic network over a larger q-range that may include further deformation modes. This phenomenon should be the subject of a dedicated study combining real-space imaging and scattering studies. Such additional relaxation may lead to the underestimation of the hydrodynamic radius of the capsules. However, we could confirm that the general linear dependence of the decay rate, Γ, versus q^2 was respected, confirming the validity of the approach. As mentioned in the previous section, it is also worth noting that some of the large error bars observed for the determination of the hydrodynamic radius are related to the size and form factor of the capsules. Measuring through form factor minima may then lead to significant variations in the measured diffusion coefficient depending on the size polydispersity.[4]

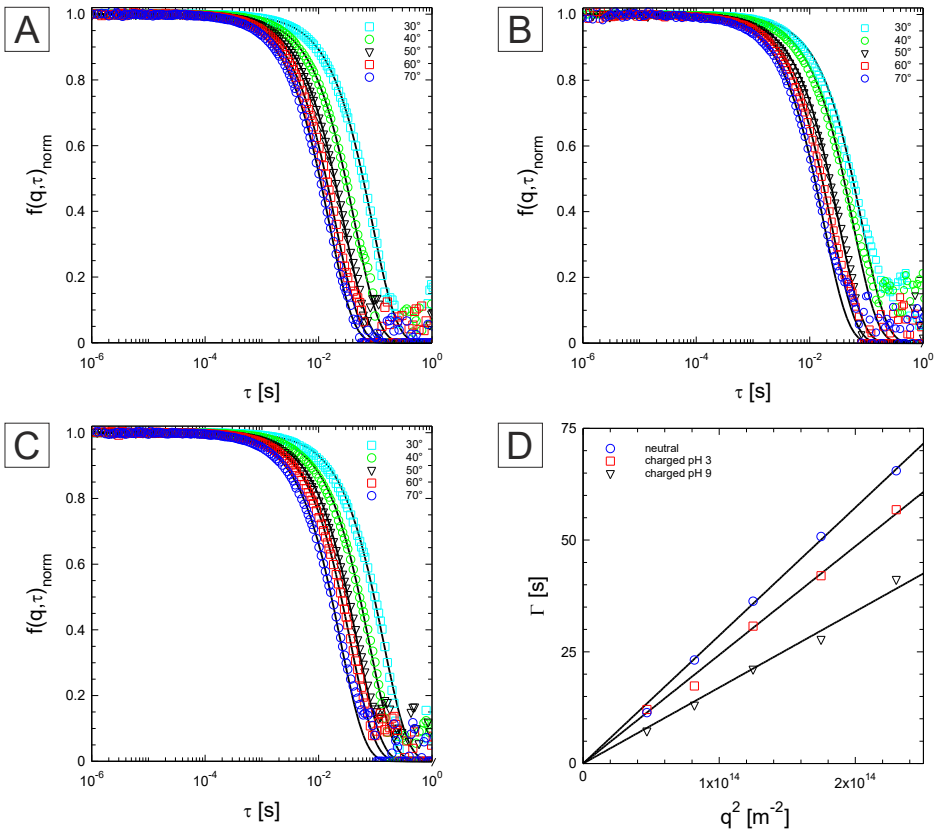

Figure S6 Normalized intermediate scattering functions (symbols) measured from 30 to 70° at 20°C on a dilute dispersion of neutral microgels capsules (A), charged microgel capsules (pH = 3, I = 1 mM) (B) and charged microgel capsules (pH = 9, I = 1 mM) (C). The data are fitted with a first cumulant analysis (full lines). (D) Plot of the decay rate, Γ as function of the squared scattering vector, q^2 for the three different systems (symbols). The diffusion coefficient was determined from the linear regression, $\Gamma = Dq^2$ (full lines).

S5 Buckling behaviour: pH jump experiments

Additional buckling experiments were performed on the P(NIPAM-co-IA) microgel capsules, as detailed in the experimental section of the main manuscript. To verify the reversibility of the buckling process discussed in Figure 9 of the main manuscript, a dilute dispersion of P(NIPAM-co-IA) microgel capsules was prepared in double-distilled water containing 10 wt% dextran. The pH was then adjusted from basic to acidic and back by the addition of sodium hydroxide (NaOH) and hydrochloric acid (HCl) solutions. Each addition was made after one hour of equilibration. From these experiments, we observed the reversible buckling of the capsules with pH, determined from the statistical analysis of the fraction of buckled particles, f_B. These experiments demonstrate that under such conditions, the dextran molecules were not able to significantly diffuse through the microgel shell. A more detailed characterization of the capsules' permeability, depending on the degree of deprotonation, ionic strength, and osmolite molecular weight, will be undertaken in the future. It is worth noting that the dimensions of the capsules strongly depend on the ionic strength, as shown by the difference between Figure S7A and C.

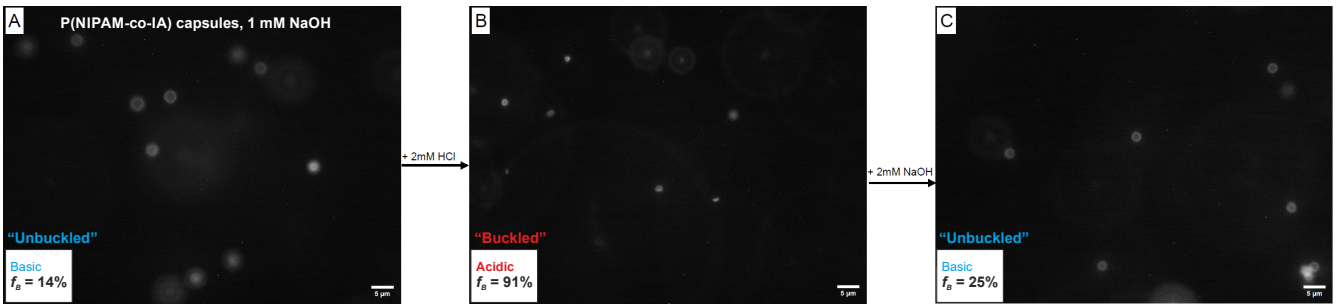

Figure S7 Fluorescent micrographs of the P(NIPAM-co-IA) microgel capsules dispersed in double-distilled water with 10 wt% dextran at 22 °C after the addition of 1 mM NaOH (basic conditions) (A). Under such conditions, most of the capsules are well-dispersed and spherical (f_B = 14 %). (B) Buckling transition occurs when 2 mM HCl (acidic conditions) is added to the former samples. Most of the capsules present a buckled conformation (f_B = 91 %). (C) Switching back to basic conditions by the addition of 2 mM NaOH, most of the capsules recover their spherical conformation (f_B = 25 %).

S6 Supporting Videos

Video S1. Video of the diffusing neutral hollow microgels from fluorescence microscopy.
Video S2. Video of the diffusing charged hollow microgels (at pH = 9) from fluorescence microscopy.
Video S3. CLSM video of a charged hollow microgels (at pH = 9) showing its thermally activated shape fluctuations.

References

1 P. J. Lu, F. Giavazzi, T. E. Angelini, E. Zaccarelli, F. Jargstorff, A. B. Schofield, J. N. Wilking, M. B. Romanowsky, D. A. Weitz and R. Cerbino, *Phys. Rev. Lett.*, 2012, **108**, 218103.

2 F. Hagemans, F. Camerin, N. Hazra, J. Lammertz, F. Dux, G. Del Monte, O.-V. Laukkanen, J. J. Crassous, E. Zaccarelli and W. Richtering, *ACS Nano*, 2023, **17**, 7257–7271.

3 P. Brocca, L. Cantù, M. Corti, E. Del Favero and S. Motta, *Langmuir*, 2004, **20**, 2141–2148.

4 G. Bryant, S. Martin, A. Budi and W. van Megen, *Langmuir*, 2003, **19**, 616–621.